Ab initio quantum mechanical gas phase and reaction field solvation study on the proton abstraction from hydroxyacetaldehyde by formate: implications for enzyme catalysis

Mikael Peräkylä

Department of Chemistry, University of Joensuu, PO Box 111, FIN-80101, Joensuu, Finland

Proton abstraction from a model carbon acid hydroxyacetaldehyde by formate has been studied using *ab initio* quantum mechanical calculations up to the MP4(SDQ)/6-31+G//HF/6-31+G* level. Solvation effects are included using the polarisable continuum method. The calculated energies of several intermediates and transition states of the proton transfer reaction are found to be in reasonable agreement with the available experimental data. Calculations show that the α-carbon, which loses a proton in the reaction, retains a substantial amount of sp^3 character in the transition state of the reaction. Therefore the resonance-stabilised enolate anion product, in which the α-carbon is sp^2 hybridised, develops after the transition state has been passed. Inclusion of solvation energies moves the transition state to an earlier point on the reaction profile. This indicates that in the case of enzyme-catalysed reaction, in which the protein environment presumably can stabilise an enolate-like structure more efficiently than water does, the transition state would be even less enolate-like unless enzymes had other means of enhancing the reaction and making the transition state occur later. We discuss how lowering of the intrinsic reaction barrier and proton tunnelling may move the transition state of the enzyme-catalysed proton abstraction reaction to a later point on the reaction profile.**

Introduction

In contrast to fast proton transfer between two electronegative atoms (*e.g.* N, O and S) proton transfer from carbon is usually a slow reaction and has a large intrinsic barrier.[1] The reasons giving rise to these have been of much interest. They have been attributed to changes in electron delocalisation and hybridisation, poor hydrogen bond donor–acceptor properties of carbon and solvent reorganisation in the transition state.[1–3] In cases where proton abstraction produces resonance-stabilised anions there exists a lag in structural and solvational reorganisation called transition state imbalance.[4] The transition state imbalance, which is at least partially responsible for the high intrinsic barriers, originates from the fact that at the transition state the hybridisation of the carbon which donates a proton in the reaction lags behind the proton transfer.[2,4–7] Interestingly, enzymes have been found to be able to lower the activation energies for proton abstraction reactions by 40–85 kJ mol^{-1} compared to the corresponding solution reactions.[8–11] Recently the mechanisms by which enzymes activate the α-protons (adjacent to carbonyl, ester or carboxylate groups) and how enzymes can stabilise the high-energy enolate or enol intermediates formed in the proton abstraction reactions have received a lot of interest from experimental and theoretical groups.[8–16] Triosephosphate isomerase (TIM) is the most extensively experimentally and theoretically studied enzyme which catalyses carbonyl group activated abstraction of an α-proton.[17–19]

In this paper we report results from our *ab initio* quantum mechanical study of the proton abstraction from model carbon acid hydroxyacetaldehyde by formate. One water molecule was added to the quantum mechanical system in order to model specific solvation of the oxygens of hydroxyacetaldehyde. Geometries of two transition states, several possible reaction intermediates and products were optimised in the gas phase. The effect of solvation on the reaction energies was taken into account by using the polarisable continuum method. This system serves as a simple model for the α-proton abstraction from activated carbon acids in general and for the enzyme triosephosphate isomerase (TIM)-catalysed reaction, which has been investigated by several groups using computer simulation methods,[16,20–24] in particular. In this work the major emphasis is laid on the structures and gas-phase and solution-phase energies of various possible high-energy reaction intermediates and enediol and enolate products of the reaction. In addition, we compare the calculated reaction energies and available experimental data in order to assess the reliability of the computational approach used.

Computational details

The geometries of the minima (Fig. 1, **I1**–**I7**) and the transition states (**TS1** and **TS2**) of the reaction sequence studied were optimised at the HF/6-31 + G* level using the Gaussian 94 program.[25] The structures of the molecular species studied are schematically shown in Fig. 1 and discussed in more detail in the section 'Geometries and charge distributions'. The HF/6-31 + G* optimised geometries were used in single-point energy calculations at the MP2/6-31 + G**, MP3/6-31 + G** and MP4(SDQ)/6-31 + G** level and in calculating the electrostatic solvation energies at the HF/6-31 + G* level. Solvation energy calculations were carried out using the polarisable continuum method of Tomasi[26,27] as implemented in Gaussian 94 (IPCM-method).[28] In the solvent calculations the relative permittivity (ε) was set to 78.5 (water) and a value of 0.0004 e au^{-3} for the charge density was used in the determination of the solute cavity boundary.[28] Vibrational frequencies of the optimised geometries were calculated in order to confirm the nature of the stationary points and to achieve the zero-point vibrational energies (ZPE) and the thermodynamic corrections for enthalpy (ΔH) and free energy (ΔG) at 298.15 K.[29] Unscaled frequencies were used in the vibrational analyses. We chose not to scale the calculated frequencies because of the empirical nature of the correction and because it would have changed the relative energies only minimally.[30] In addition, intrinsic reaction coordinate (IRC) calculations were used to confirm that the transition state **TS1** connects the energy minima **I2** and **I3**, and that **TS2** connects the minima **I3** and **I5**. IRC pathways were calculated in mass-weighted cartesian coordinates with a step size of 0.1 $amu^{\frac{1}{2}}$ bohr.

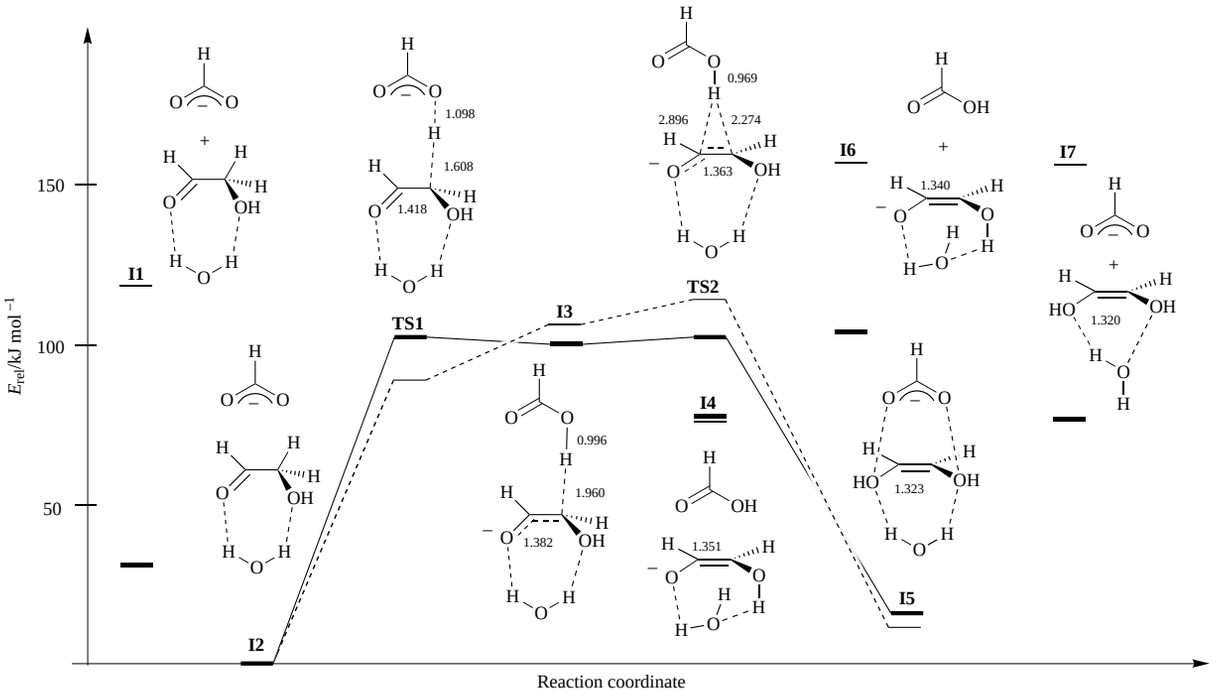

Fig. 1 Structures and relative energies [MP4(SDQ)/6-31 + G**//HF/6-31 + G* + ΔZPE] of the studied reaction sequence in the gas phase (----, thin marks) and in solution (——, thick marks)

Table 1 Total energies of the molecules[a]

	E/au			
Structure	HF/6-31 + G*	MP2/6-31 + G**	MP3/6-31 + G**	MP4(SDQ)/6-31 + G**
I1	−303.798 11	−304.664 13	−304.682 59	−304.698 36
I2	−492.049 79	−493.429 36	−493.439 67	−493.469 48
TS1[b]	−491.997 81	−493.395 45	−493.402 39	−493.430 57
I3	−491.999 26	−493.392 41	−493.401 31	−493.428 77
TS2[c]	−491.997 27	−493.388 81	−493.398 69	−493.426 09
I4	−492.007 01	−493.399 50	−493.408 95	−493.436 35
I5	−492.037 69	−493.427 29	−493.439 41	−493.465 70
I6	−303.213 42	−304.096 51	−304.106 16	−304.122 65
I7	−303.778 35	−304.652 28	−304.672 79	−304.685 68
HCOO$^-$	−188.208 19	−188.711 38	−188.708 19	−188.722 53
HCOOH	−188.769 18	−189.272 01	−189.273 10	−189.284 35

[a] Energies are calculated using geometries optimised at the HF/6-31 + G* level. Structures are shown in Fig. 1.[b] Imaginary frequency is −808.91. [c] Imaginary frequency is −161.59.

Table 2 ΔZPE, Δ*H*, and Δ*G* corrections calculated at the HF/6-31 + G* level[a]

Structure	ΔZPE/kJ mol^{-1}	Δ*H*/kJ mol^{-1}	Δ*G*/kJ mol^{-1}
I1	−10.3	−8.9	−59.3
TS1	−13.1	−15.6	−9.6
I3	−2.2	−3.2	−1.2
TS2	1.3	−3.9	1.9
I4	2.7	0.3	6.6
I5	1.5	−0.1	4.4
I6	−7.3	−7.7	−53.1
I7	−6.8	−7.1	−48.4

[a] Energies are relative to **I2**.

Results and discussion

Total energies of the minima and transition states at different computational levels are listed in Table 1 and the corrections for ΔZPE, Δ*H*, and Δ*G* in Table 2. Selected optimised geometric parameters of **I2**, **TS1**, **I3**, **TS3**, **I4** and **I5** are listed in Table 3. The relative gas-phase energies (Δ*E*) at the MP2, MP3 and MP4(SDQ) level, and the relative energies (ΔE_s), enthalpies (ΔH_s) and free energies (ΔG_s) with solvation energies included are listed in Table 4. Structures and relative energies of the reaction sequence calculated at the MP4(SDQ)/6-31 + G**//HF/6-31 + G* level both in the gas-phase (Δ*E*) and with solvation energies included (ΔE_s) are shown in Fig. 1. All the energies reported include ZPE corrections.

Geometries and charge distributions

In the hydrogen bonded formate–hydroxyacetaldehyde–water complex, **I2** (Fig. 1), one oxygen of the proton-abstracting formate makes a hydrogen bond to the hydroxy hydrogen and the other is coordinated to the α-proton of hydroxyacetaldehyde. In this complex the water molecule donates a hydrogen bond to both oxygens of hydroxyacetaldehyde. The mode of binding of water is similar to that of **I2** in **I1**, **TS1**, **I3**, **TS2** and **I5**. In the case of **I4**, **I6** and **I7** water donates one hydrogen bond to the carbonyl oxygen and accepts one from the hydroxy group of hydroxyacetaldehyde. In the transition state of the proton abstraction, **TS1**, the α-proton is almost completely transferred to formate [*r*(O–H) = 1.098 Å] and the α-carbon has retained the tetrahedral geometry of an sp^3 carbon. This can be seen from the value of the CH(OH) angle, which is the angle between Cl–C2 axis and bisector OH–C2–H3. In **TS1** the CH(OH) angle is 136.0°, slightly larger than 123.5° of the tetrahedral α-carbon of **I2** [CH(OH) angle is 180° for a planar structure]. In general the geometry and charge distribution of

Table 3 Selected geometric parameters of **I2**, **TS1**, **I3**, **TS2**, **I4** and **I5** optimised at the HF/6-31 + G* level[a]

	Distance/Å						Angle/°		
Structure	O1–C1	C1–C2	C2–H2	C2–O_f	O1–H_w	H2–O_f	C1–C2–H2	C2–H2–O_f	O1–H_w–O_w
I2	1.230	1.517	1.097	2.952 3.279	2.205	2.594 3.167	107.39	86.01 97.93	140.22
TS1	1.223	1.418	1.608	2.703	2.071	1.098	103.14	173.92	150.31
I3	1.243	1.382	1.960	2.954	1.976	1.000	92.65	172.45	156.05
TS2	1.263	1.363	2.274	3.312	1.928	0.969	69.47	162.62	158.24
I4	1.272	1.351	2.563	3.442	1.794	0.986	109.43	148.38	164.34
I5	1.354	1.323			2.211	1.735			147.49

[a] See text for the numbering of hydroxyacetaldehyde. O_f is formate oxygen, O_w is water oxygen, and H_w is water hydrogen.

TS1 are similar to the corresponding parameters in the transition states of the proton abstraction from acetaldehyde by the first-row hydride anions NH_2^-, OH^- and F^-.[6]

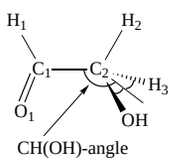

IRC calculations (HF/6-31 + G*) showed that **TS1** connects minima **I2** and **I3**. In **I3** the transferred proton is hydrogen bonded to the α-proton [*r*(C2–H2) = 1.96 Å] which has partly retained tetrahedral geometry. CH(OH) angle is 152.5° in **I3** and α-carbon still possesses a large negative partial charge (see below). The hydrogen bonding interaction seen in **I3**, and a similar interaction in **TS1**, is believed to play a major role in lowering the energy of this structure and the barrier for proton transfer in the gas phase.[5,6,31] The stabilising interaction comes from the favourable electrostatic interaction between the negative charge on the α-carbon, the positive charge on the proton that is transferred and the negative charge on the proton accepting atom (carboxylate oxygen). For example, in **TS1** the Mulliken charge on the α-carbon is −0.43 (charge obtained from natural bond orbital analysis[32,33] is −0.34), on the proton it is 0.48 (0.49) and on carboxylate oxygen it is −0.69 (−0.81). Thus, the three atoms form a '− + −' charge system which strongly stabilises this structure. The fact that the α-carbon has only partially changed hybridisation from sp^3 to sp^2 in **TS1** and **I3** indicates that the geometrical change and the formation of a resonance-stabilised enolate anion is lagging behind the proton transfer. In addition, it has been shown earlier that the formation of sp^2 carbon is needed before the resonance-stabilised enolate anion can be formed and that this is the underlying reason why transition state imbalance is observed in this kind of reactions.[4,6] From **I3** the proton abstraction reaction can go on to **TS2** or **I4**. **TS2** is a transition state which connects (conformed by IRC calculations) **I3** and enediol **I5**. At **TS2** the transferred proton is bonded to formate's oxygen [*r*(O–H) = 0.97 Å) and is located above the π-electron cloud of the partial double bond and between the two carbons of hydroxyacetaldehyde. The hydrogen to carbon distances are 2.90 (H2–C1) and 2.27 Å (H2–C2) in this structure. From enolate **I4** the proton abstraction reaction can go on to **I5** by the proton transfer from formate to the anionic oxygen of hydroxyacetaldehyde (O1) or to **I6** by the separation of formate and the hydroxyacetaldehyde–water complex.

The development of the proton abstraction reaction can be followed by monitoring the build-up of negative charge on CHO group (atoms H1, C1, O1) of hydroxyacetaldehyde. As the reaction progresses the carbon which loses the proton in the reaction changes hybridisation from sp^3 to sp^2, allowing the negative charge to spread from the α-carbon end of the molecule to the CHO end. This phenomenon, which has been earlier demonstrated in the case of proton transfer from acetaldehyde to its enolate ion[2] and in the case of proton abstraction from acetaldehyde by the first- and second-row hydride anions,[6] is clearly seen here as well. The charges (Mulliken charges, gas phase, HF/6-31 + G*) on the CHO group of hydroxyacetaldehyde are −0.04, −0.28, −0.41, −0.65 and −0.64 in **I2**, **TS1**, **I3**, **TS2** and **I4**, respectively, showing the expected increase in the CHO group charge as the reaction progresses. The increase in the negative charge of the CHO group indicates that the hydrogen-bonding interaction between the carbonyl oxygen and the water molecule increases as well. Since in general the strength of a hydrogen bond increases as the hydrogen-bonding distance decreases and the X–H···Y (where X and Y are electronegative atoms) angle increases, the hydrogen bonding parameters listed in Table 3 can be used as indicators of the hydrogen bond strength. From Table 3 we can see that distance O1–H_w decreases and angle O1–H_w–O_w increases in the series of **I2**, **TS1**, **I3**, **TS2** and **I4**, indicating increasing strength of the hydrogen bond. In the active sites of the proton abstraction catalysing enzymes there usually are hydrogen bond donors bonded to the enolic oxygen (O1). For example, in the case of triosephosphate isomerase, whose catalytic reaction the present system models, has histidine, lysine and asparagine in its active site, donating hydrogen bonds to the substrate's oxygen.[17] Thus, similarly to the simple model studied here, we can expect that the strength of the hydrogen bonds in the enzyme active site increases as the reaction goes on.

Energies in the gas-phase and aqueous solution

In the gas-phase the most stable (Δ*E*, Δ*H* and Δ*G*) species of the studied reaction sequence is **I2** (Fig. 1, Table 4). When solvation energies are included the energies (ΔE_s) and enthalpies (ΔH_s) are also the most stable for **I2**, but the free energy (ΔG_s) of **I1** is 17.1 kJ mol^{-1} smaller than that of **I2**. This change in stability is a result of more favourable solvation energies of the species in which the hydroxyacetaldehyde–water complex and formate or formic acid are (infinitely) separated (**I1**, **I6** and **I7**) and the contribution of the favourable rotational and translational entropy on the free energies of such species. However, it must be noted that, because the rotational and especially translational motions are more restricted in aqueous phase than in the gas-phase, the corrections applied here in estimating the entropy change are overestimates of the true values. In the gas-phase **TS1** is 89.1 kJ mol^{-1} more unstable than **I2** at the MP4(SDQ)/6-31 + G**//HF/6-31 + G* + ΔZPE level. Intermediate **I3**, which is a local minimum at the HF/6-31 + G* level, is 15.6 kJ mol^{-1} and the transition state **TS2** is 23.5 kJ mol^{-1} less stable than **TS1** when effects of electron correlation [MP4(SDQ)] and ΔZPE energies are included. However, since **I3** and **TS2** are solvated better than **TS1** the energy of **I3** is lower than that of the transition states **TS1** and **TS2** in the aqueous phase. This is due to the fact that the negative charge is localised in the tetrahedral α-carbon in **TS1** but in **TS2** and **I3** the negative charge is spread to the CHO group of hydroxyacetaldehyde, increasing the solvation energy. In the gas-phase the enolate intermediate **I4** is calculated to be 29.0 kJ mol^{-1}

Table 4 Relative energies (ΔE) of the studied species at various levels in the gas-phase and relative energies (ΔE_s), enthalpies (ΔH_s) and free energies (ΔG_s) with the solvation energies included[a]

	ΔE/kJ mol^{-1}			ΔE_s/kJ mol^{-1}	ΔH_s/kJ mol^{-1}	ΔG_s/kJ mol^{-1}
	MP4(SDQ)	MP3	MP2	MP4(SDQ)	MP4(SDQ)	MP4(SDQ)
I1	117.2	118.0	131.1	31.1	32.5	−17.1
TS1	89.1	84.8	76.0	101.5	99.0	100.7
I3	104.7	98.5	94.8	98.4	97.3	93.2
TS2	112.6	106.3	105.2	102.4	99.8	99.2
I4	75.7	78.0	84.3	76.4	74.0	82.6
I5	11.4	2.1	6.9	16.1	14.5	9.7
I6	156.7	151.3	152.4	104.4	104.1	53.2
I7	154.1	147.3	165.7	75.8	75.5	27.4

[a] ΔZPEs are included in the energies. HF/6-31 + G* optimised geometries were used. Energies are relative to **I2**. 6-31 + G** basis set was used in the Møller–Plesset calculations.

Table 5 Comparison of the experimental (ΔG_{exp}) and calculated (ΔG_{calc}) (MP4/6-31 + G**//HF/6-31 + G* + ΔZPE + ΔE_{solv}) free-energies[a]

Reaction	ΔG_{exp}/kJ mol^{-1}	ΔG_{calc}/kJ mol^{-1}
1 **I1**→**I6**	74.0	70.3
2 **I1**→**I7**	35.5	44.5
3 **I6**→**I7**	38.5	25.8
4 **I1**→**TS1**	105	117.8

[a] See text for the estimation of experimental energies.

more stable than **I3** and 36.9 kJ mol^{-1} more stable than **TS2**. The relative energies of these three species are only slightly affected by the solvation energies. ΔG_s of **I6**, which is otherwise similar to **I4** except that formic acid is separated from the hydroxyacetaldehyde–water complex, is 29.4 kJ mol^{-1} more stable than **I4** and ΔG_s for the complexation of formate and enediol of hydroxyacetaldehyde (**I7**→**I5**) is calculated to be 17.7 kJ mol^{-1} in solution. These values are the calculated complexation free-energies of the two dimers.

Comparison of the calculated and experimental energies

Comparison of the experimental and calculated aqueous phase free energies of several subreactions of the reaction sequence (Fig. 1) are listed in Table 5 (reactions 1–4). Because the experimental reaction energies are calculated from the pK_a values ($\Delta\Delta G = 2.3RT\delta pK_a$) of CH_3CHO (pK_a of the α-proton is 16.7), CH_2=COH (pK_a of the hydroxyl proton is 10.5)[34] and HCOOH (pK_a is 3.75)[35] the values in Table 5 are only estimates of the true ones. The transition state energy of the proton abstraction reaction (reaction 4 in Table 5) has been estimated using the linear free energy relationship between the reaction rate (and the transition state energy through the use of the transition state theory) and the ΔpK_a between the proton abstracting base and carbon acid using the data from the paper of Åqvist and Fothergill.[21] The data in Table 5 show that in spite of the use of a simplified continuum reaction field description of solvent, the use of gas-phase structures in estimating the solvation energies, and the use of gas-phase thermodynamic corrections the agreement between the experiment and theory is encouraging. We can conclude that these kind of simple calculations can give at least a qualitative picture of the proton abstraction reaction in aqueous solution.

Implications for enzyme catalysis

There has been a lot of discussion of how enzymes accelerate the proton abstraction reaction and stabilise the high-energy enolate or enol intermediates formed in the reaction. It has been suggested that this stabilisation is provided either by electrostatic stabilisation of the enolate (or enolate-like transition state),[14,36] or by the formation of a short, strong hydrogen bond between the negatively charged enolate oxygen and an active-site amino acid, which functions as a hydrogen bond donor.[11,13] In addition to the stabilisation of the enolate intermediate, which lowers the thermodynamic barrier of the reaction, it has been suggested that in order to reach the observed reaction rate enhancement enzymes need to lower the intrinsic reaction barrier as well.[10] This most probably is the case because enzyme active sites are preorganised to stabilise enolate intermediates, whereas in solution the stabilisation of the enolate involves considerable solvent reorganisation. Thus the intrinsic barrier in enzyme reaction is lower mainly due to the more favourable entropy term. Although the stabilisation of the enolate intermediate moves the transition state of the enzyme reaction to an earlier point on the reaction surface (based on the Hammond postulate[37]), the lowering of the intrinsic barrier acts in the opposite direction resulting in a transition state which is thought to be late.[10] A late transition state makes it possible that enzyme can more efficiently take advantage of the stabilisation provided by the active-site amino acids. This conclusion comes from the fact that as the proton abstraction reaction proceeds the anionic oxygen of the carbon acid becomes increasingly more negative. This evidently increases the stabilisation provided by the enzyme environment.

The calculations presented here show that in aqueous phase the structure with the enolate-like carbon acid, **I4**, is clearly more stable than **TS1** and, therefore, at the calculated transition state the enolate anion is not fully formed. Since negative charge has spread much less to the CHO end of the molecule in **TS1** than in **I4**, the latter species is more stabilised by the solvation energies. Consequently, this leads to an earlier transition state in the aqueous phase than in the gas phase. Furthermore, it is reasonable to assume that this stabilisation would be more pronounced in enzyme active sites, leading to an earlier transition state than in aqueous solution. However, this would be in contrast to the assumption that transition states in enzyme-catalysed proton abstraction reactions are late and strongly stabilised by the active-site interactions. As mentioned above, the preorganised enzyme active site is probably important in lowering the intrinsic reaction barrier. Another factor which can make the transition state occur later is tunnelling of the proton. Proton tunnelling may be important in lowering the energy of the part of the reaction where the proton is transferred from the α-carbon to the carboxylate oxygen (from **I2** to **TS1** in Fig. 1). This would help moving the transition state to a later point on the reaction profile where the enzyme can more efficiently stabilise the transition state and the formed enolic intermediate. This interpretation has support from experimental data on enzyme-catalysed and non-catalysed proton abstraction reactions.[38] These data indicate that there exist tunnelling in non-catalysed proton abstraction reactions and it probably plays a more important role in enzyme-catalysed than non-catalysed reactions. Furthermore, as discussed recently by Alston *et al.*,[38] proton tunnelling may be important in lowering the barrier for the proton transfer in the triosephosphate

isomerase-catalysed reaction and be a general feature in enzymatic proton abstraction reactions. Although it seems probable that both the lowering of the intrinsic barrier and proton tunnelling play an important role in enzyme-catalysed proton abstraction, the magnitude of these factors are as yet unknown.

Conclusions

In this work we studied proton abstraction from a model carbon acid hydroxyacetaldehyde by formate using *ab initio* quantum mechanical calculations up to the MP4(SDQ)/6-31 + G**//HF/6-31 + G* + ΔZPE level. Solvation effects were included using the polarisable continuum method. Comparison of the calculated energies of several intermediates and the transition state of the proton abstraction and the available experimental data showed that in spite of several simplifications in the calculations the agreement with the experiments was reasonable.

Proton abstraction from a carbon acid studied here, like such reactions in general, is characterised by transition state imbalance. This means that at the transition state charge delocalisation and geometrical changes of the carbon acid lag behind the proton transfer. Consequently, the formation of the resonance-stabilised enolate anion of hydroxyacetaldehyde lags behind the proton transfer. Because of this the minima, which are located after the transition state of the proton transfer step, **TS1**, are stabilised more by the solvation than the transition state. This leads, according to the Hammond postulate, to an earlier transition state in aqueous phase than in the gas phase. In addition, it is probable that in the case of enzyme-catalysed proton abstraction the active-site amino acids and protein environment stabilise the forming enolate at least as well as the aqueous environment. However, since in the enzymatic proton abstraction reaction the transition state is believed to be late, enzymes must be able to lower the intrinsic reaction barrier of the reaction in order to fulfil this requirement. This can be accomplished by the stabilisation of the transition state and enolic intermediate by the preorganised enzyme active site and by enhanced proton tunnelling.

References

1 R. P. Bell, *The Proton in Chemistry*, Chapman and Hall, London, 1973.
2 C. F. Bernasconi and P. J. Wenzel, *J. Am. Chem. Soc.*, 1994, **116**, 5405.
3 C. F. Bernasconi, *Acc. Chem. Res.*, 1992, **25**, 9.
4 C. F. Bernasconi, *Adv. Phys. Org. Chem.*, 1992, **27**, 119.
5 C. F. Bernasconi, P. J. Wenzel, J. R. Keeffe and S. Gronert, *J. Am. Chem. Soc.*, 1997, **119**, 4008.
6 M. Peräkylä, *J. Phys. Chem.*, 1996, **100**, 3441.
7 W. H. Saunders, Jr., *J. Am. Chem. Soc.*, 1994, **116**, 5400.
8 J. A. Gerlt and P. G. Gassman, *J. Am. Chem. Soc.*, 1992, **114**, 5928.
9 J. A. Gerlt, J. W. Kozarich, G. L. Kenyon and P. G. Gassman, *J. Am. Chem. Soc.*, **113**, 9667.
10 J. A. Gerlt and P. G. Gassman, *J. Am. Chem. Soc.*, 1993, **115**, 11 552.
11 J. A. Gerlt and P. G. Gassman, *Biochemistry*, 1993, **32**, 11 943.
12 W. W. Cleland and M. M. Kreevoy, *Science*, 1994, **264**, 1887.
13 P. A. Frey, S. A. Whitt and J. B. Tobin, *Science*, 1994, **264**, 1927.
14 A. Warshel, A. Papazyan and P. A. Kollman, *Science*, 1995, **269**, 102.
15 S. Scheiner and T. Kar, *J. Am. Chem. Soc.*, 1995, **117**, 6970.
16 G. Alagona, C. Ghio and P. A. Kollman, *J. Am. Chem. Soc.*, 1995, **117**, 9855.
17 M. E. M. Noble, R. K. Wierenga, A.-M. Lambeir, F. R. Opperdoes, A.-M. W. H. Thunnissen, K. H. Kalk, H. Groendijk and W. G. J. Hol, *Proteins*, 1991, **10**, 50.
18 J. D. Hermes, S. C. Blacklow and J. R. Knowles, *Proc. Natl. Acad. Sci. USA*, 1990, **87**, 696.
19 J. R. Knowles and W. J. Albery, *Acc. Chem. Res.*, 1977, **10**, 105.
20 M. Peräkylä and T. A. Pakkanen, *Proteins*, 1996, **25**, 225.
21 J. Åqvist and M. Fothergill, *J. Biol. Chem.*, 1996, **271**, 10 010.
22 M. Peräkylä, *J. Chem. Soc., Chem. Commun.*, 1996, 361.
23 P. A. Bash, M. J. Field, R. C. Davenport, G. A. Petsko, D. Ringe and M. Karplus, *Biochemistry*, 1991, **30**, 5826.
24 V. Daggett, F. Brown and P. Kollman, *J. Am. Chem. Soc.*, 1989, **111**, 8247.
25 M. J. Frisch, G. W. Trucks, H. B. Schlegel, P. M. W. Gill, B. G. Johnson, M. A. Robb, J. R. Cheeseman, T. A. Keith, G. A. Peterson, J. A. Montgomery, K. Rachavachiri, M. A. Al-Laham, V. G. Zakrzewski, J. V. Oritz, J. B. Foresman, J. Cioslowski, B. B. Stefanov, A. Nanayakkara, M. Challacombe, C. Y. Peng, P. Y. Ayala, W. Chen, M. W. Wong, J. L. Andres, E. S. Replogle, R. Gomperts, R. L. Martin, D. J. Fox, J. S. Binkley, D. J. Defrees, J. Baker, J. J. P. Stewart, M. Head-Gordon, C. Gonzales and J. A. Pople, GAUSSIAN 94 (Revision B.3), Gaussian, Inc. Pittsburgh, PA, 1995.
26 J. Tomasi and M. Persico, *Chem. Rev.*, 1994, **94**, 2027.
27 S. Miertus, E. Scrocco and J. Tomasi, *Chem. Phys.*, 1981, **55**, 117.
28 K. B. Wiberg, P. R. Rablen, D. J. Rush and T. A. Keith, *J. Am. Chem. Soc.*, 1995, **117**, 4261.
29 W. J. Hehre, L. Radom, P. von Rague Schleyer and J. A. Pople, *Ab Initio Molecular Orbital Theory*, Wiley, New York, 1986.
30 A. Rastelli, M. Bagatti and R. Gandolfi, *J. Am. Chem. Soc.*, 1995, **117**, 4965.
31 S. Gronert, *J. Am. Chem. Soc.*, 1993, **115**, 10 258.
32 A. E. Reed, R. B. Weinstock and F. Weinhold, *J. Chem. Phys.*, 1985, **83**, 735.
33 J. P. Foster and F. Weinhold, *J. Am. Chem. Soc.*, 1989, **102**, 7211.
34 *The Chemistry of Enols*, ed. Z. Rappoport, Wiley, New York, 1990.
35 *Lange's Handbook of Chemistry*, McGraw-Hill, London, 1979.
36 J. P. Guthrie and R. Kluger, *J. Am. Chem. Soc.*, 1993, **115**, 11 569.
37 G. S. Hammond, *J. Am. Chem. Soc.*, 1955, 77, 334.
38 W. C. Alston, II, M. Kanska and C. J. Murray, *Biochemistry*, 1996, **35**, 12 873.

Paper 7/04021K
Received 9*th June* 1997
Accepted 9*th July* 1997